Cell

The Oxygen-Rich Postnatal Environment Induces Cardiomyocyte Cell-Cycle Arrest through DNA Damage Response

Bao N. Puente,[1,3,12] Wataru Kimura,[1,12] Shalini A. Muralidhar,[1] Jesung Moon,[3] James F. Amatruda,[1,2,3] Kate L. Phelps,[4] David Grinsfelder,[5] Beverly A. Rothermel,[1,2] Rui Chen,[1] Joseph A. Garcia,[1] Celio X. Santos,[7] SuWannee Thet,[1] Eiichiro Mori,[6] Michael T. Kinter,[8] Paul M. Rindler,[8] Serena Zacchigna,[9] Shibani Mukherjee,[6] David J. Chen,[6] Ahmed I. Mahmoud,[11] Mauro Giacca,[9] Peter S. Rabinovitch,[10] Asaithamby Aroumougame,[6] Ajay M. Shah,[7] Luke I. Szweda,[8] and Hesham A. Sadek[1,*]

[1]Department of Internal Medicine
[2]Department of Molecular Biology
[3]Department of Pediatrics
[4]Department of Cell Biology
[5]Department of Clinical Science
[6]Department of Radiation Oncology
The University of Texas Southwestern Medical Center, Dallas, TX 75390, USA
[7]Cardiovascular Division, King's College London BHF Centre of Research Excellence, School of Medicine, James Black Centre, London SE5 9NU, UK
[8]Free Radical Biology and Aging Research Program, Oklahoma Medical Research Foundation, Oklahoma City, OK 73104, USA
[9]Molecular Medicine Laboratory, International Centre for Genetic Engineering and Biotechnology, 34149 Trieste, Italy
[10]Department of Pathology, University of Washington, Seattle, WA 98195, USA
[11]Cardiovascular Division, Department of Medicine, Brigham and Women's Hospital and Harvard Medical School, Cambridge, MA 02115, USA
[12]Co-first author
*Correspondence: hesham.sadek@utsouthwestern.edu
http://dx.doi.org/10.1016/j.cell.2014.03.032

SUMMARY

The mammalian heart has a remarkable regenerative capacity for a short period of time after birth, after which the majority of cardiomyocytes permanently exit cell cycle. We sought to determine the primary postnatal event that results in cardiomyocyte cell-cycle arrest. We hypothesized that transition to the oxygen-rich postnatal environment is the upstream signal that results in cell-cycle arrest of cardiomyocytes. Here, we show that reactive oxygen species (ROS), oxidative DNA damage, and DNA damage response (DDR) markers significantly increase in the heart during the first postnatal week. Intriguingly, postnatal hypoxemia, ROS scavenging, or inhibition of DDR all prolong the postnatal proliferative window of cardiomyocytes, whereas hyperoxemia and ROS generators shorten it. These findings uncover a protective mechanism that mediates cardiomyocyte cell-cycle arrest in exchange for utilization of oxygen-dependent aerobic metabolism. Reduction of mitochondrial-dependent oxidative stress should be an important component of cardiomyocyte proliferation-based therapeutic approaches.

INTRODUCTION

The pathophysiological basis of heart failure is the inability of the adult heart to regenerate lost or damaged myocardium, and although limited myocyte turnover does occur in the adult heart, it is insufficient for restoration of contractile dysfunction (Bergmann et al., 2009; Hsieh et al., 2007; Laflamme et al., 2002; Nadal-Ginard, 2001; Quaini et al., 2002). In contrast, the neonatal mammalian heart is capable of substantial regeneration following injury through cardiomyocyte proliferation (Porrello et al., 2011b, 2013), not unlike urodele amphibians (Becker et al., 1974; Flink, 2002; Oberpriller and Oberpriller, 1974) or teleost fish (González-Rosa et al., 2011; Poss et al., 2002; Wang et al., 2011). However, this regenerative capacity is lost by postnatal day 7 (Porrello et al., 2011b, 2013), which coincides with cardiomyocyte binucleation and cell-cycle arrest (Soonpaa et al., 1996). Although several regulators of cardiomyocytes cell cycle postnatally have been identified (Bersell et al., 2009; Chen et al., 2013; Eulalio et al., 2012; Mahmoud et al., 2013; Porrello et al., 2011a; Sdek et al., 2011; Xin et al., 2013), the upstream signal that causes permanent cell-cycle arrest of most cardiomyocytes remains unknown.

One of many factors shared by organisms that are capable of heart regeneration is the oxygenation state. For example, the zebrafish's stagnant and warm aquatic environment has 1/30th oxygen capacitance compared to air and is prone to poor oxygenation, which may explain the remarkable tolerance of

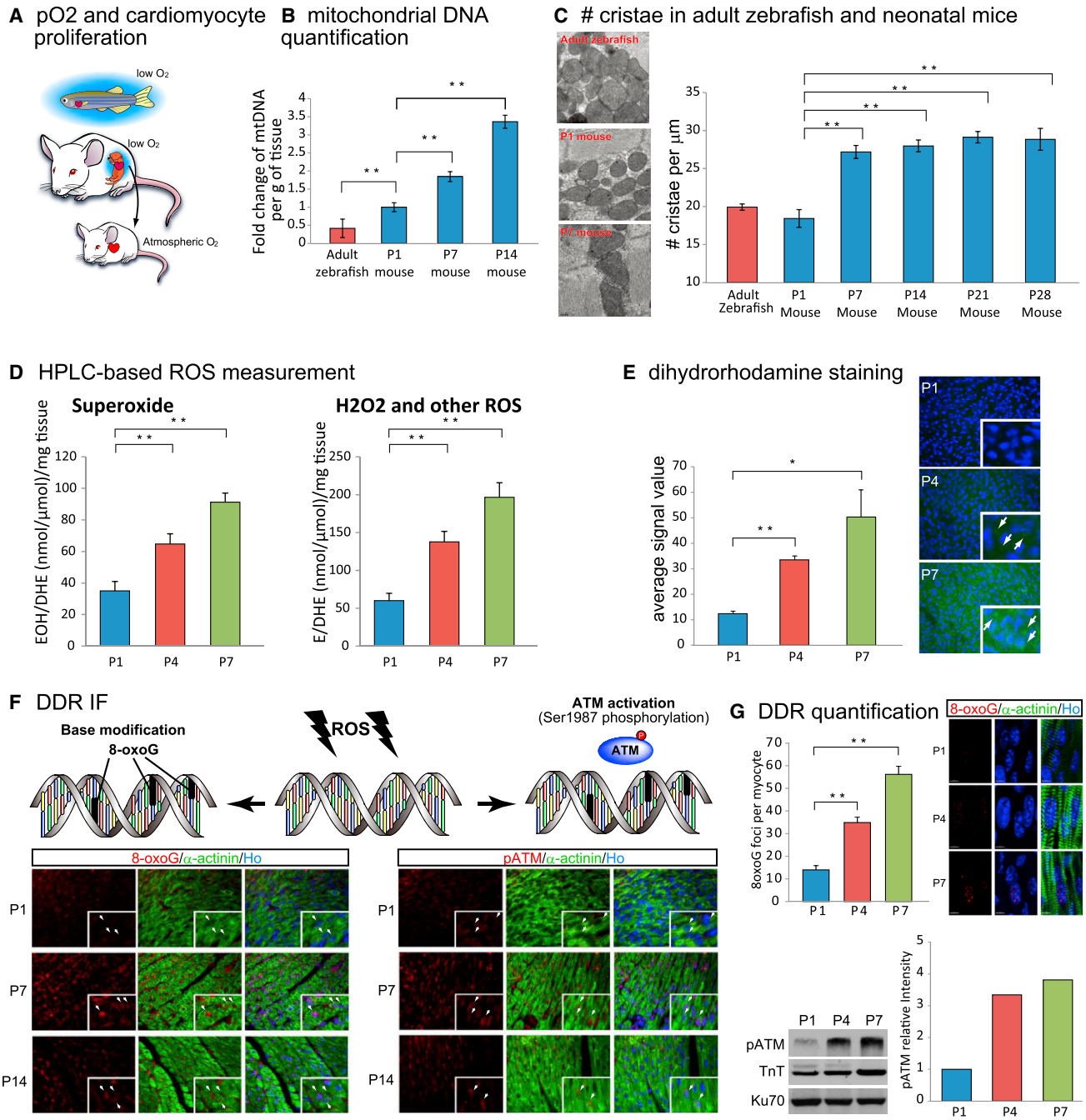

Figure 1. Oxidation State, Activity of Mitochondrial Respiration, Oxidative Stress, and the Activation of DNA Damage Response Correspond to Cardiac Regenerative Capacity

(A) Fishes and mammalian fetuses are under low-oxygenated environment, whereas postnatal mammals are in well-oxygenated atmosphere.

(B) qRT-PCR analysis revealed postnatal increase in mitochondrial DNA (mtDNA) contents per gram of tissue (ventricles) until postnatal day 14 (P14). Relative mtDNA content in adult zebrafish was even smaller than that in P1 mouse.

(C) TEM images of ventricles showed more mature cristae structure in P7 mouse heart comparing with P1 mouse heart and adult zebrafish heart (left). The number of mitochondrial cristae counted from SEM images increased in P7 mouse heart compared to P1 mouse heart (table, blue bars) and also to adult zebrafish heart (table, red bar).

(D) HPLC detection of a superoxide probe dihydroethidium (DHE) revealed a significant increase in both 2-hydroxyethidium (EOH), a specific product for superoxide anion radical, and in ethidium (E), oxidized by other reactive oxygen species such as H_2O_2 (mainly) and ONOO from P1 to P7.

(E) Imaging of ROS on cryosections with dihydrorhodamine 123 staining indicated linear increase in cardiomyocyte ROS level from P1 to P7 (arrows).

(F) Immunostaining with oxidative DNA damage and DNA damage response (DDR) markers. A marker for oxidative base modification in DNA, 8-oxo-7,8-dihydroguanine (8-oxoG, left panels), and for activation of DDR, Ser1987 phosphorylated ATM (pATM, right panels) were not detected in cardiomyocyte nuclei at P1

(legend continued on next page)

zebrafish to hypoxia (Rees et al., 2001; Roesner et al., 2006). Typical air-saturated water has a PaO_2 of 146 mm Hg and zebrafish can tolerate hypoxia at PaO_2 of 15 mm Hg (10% air-saturation) for 48 hr and even 8 mm Hg with hypoxic preconditioning. Moreover, the zebrafish circulatory system is relatively hypoxemic, as it has a primitive two-chamber heart with one atrium and one ventricle, which results in mixing of arterial and venous blood.

The mammalian heart has four chambers with no mixing of arterial and venous blood; however, during intrauterine life, the mammalian fetal circulation is shunt-dependent with significant arteriovenous mixing of arterial and venous blood. Mixing and shunting of blood occurs at three sites: the ductus venosus, foramen ovale, and ductus arteriosus. Blood in the umbilical vein going to the fetus is 80%–90% saturated with a PaO_2 of 32–35 mm Hg whereas the fetal venous blood return is quite desaturated at 25%–40%. Despite preferential streaming of blood through the shunts to preserve the most oxygenated blood for the brain and the myocardium, the saturation of the blood ejected from the left ventricle is only 65% saturated with a PaO_2 of 25–28 mm Hg (Dawes et al., 1954). Therefore, both the zebrafish heart and the mammalian fetal heart reside in relatively hypoxic environments (Figure 1A).

Transition from embryonic- to postnatal circulation soon after birth drastically changes the oxygenation state of cardiomyocytes. For example, arterial pO_2 increases from 30 mm Hg (Lawrence et al., 2008; Mitchell and Van Kainen, 1992; Reynolds et al., 1996) to 100 mm Hg (Webster and Abela, 2007) (Figure 1A). In parallel, energy metabolism of the embryonic and adult heart is quite distinct. During embryonic development, when cardiomyocytes rapidly proliferate, the relatively hypoxic embryonic heart utilizes anaerobic glycolysis as a main source of energy (Fisher et al., 1980; Lopaschuk et al., 1992), whereas adult cardiomyocytes utilize the oxygen-dependent mitochondrial oxidative phosphorylation as an energy source (Gertz et al., 1988; Wisneski et al., 1985). Nevertheless, the time frame of this metabolic shift and its relation to cardiomyocyte cell cycle is unknown.

Mitochondrial oxidative phosphorylation produces 18 times as much ATP as cytoplasmic glycolysis (Dismukes et al., 2001; Semenza, 2007). However, the energy advantage of mitochondrial oxidative phosphorylation over glycolysis is not without deleterious consequences, as the mitochondrion is considered the major source of free radical production (Miquel et al., 1980; Turrens, 1997, 2003). Mitochondrial ROS are generated as a consequence of electron leak by the electron transport chain (Koopman et al., 2010; Rudolph and Heyman, 1974) and can cause cellular toxicity by promoting damage of proteins, nucleic acids, lipids, or DNA, such as oxidized base, single- or double-strand breaks, resulting in cell-cycle arrest, apoptosis, or cellular senescence (Hoeijmakers, 2009; Marnett et al., 2003; Moos et al., 2000). The role of mitochondrial ROS or DNA damage response in postnatal cell-cycle arrest of cardiomyocytes is unknown.

Here, we show that early postnatal mouse and zebrafish hearts share a low mitochondrial content and complexity and lack markers of DNA damage response, all of which significantly increase in the postnatal mouse heart within days after birth. Moreover, we show that there is a temporal shift from glycolytic to oxidative metabolism, with a subsequent increase in mitochondrial ROS production, which induces cardiomyocyte cell-cycle arrest through activation of the DNA damage response. Systemic scavenging of ROS, specific scavenging of mitochondrial ROS in cardiomyocytes, or inhibition of the DNA damage response pathway all delay postnatal cell-cycle arrest of cardiomyocytes. These findings identify ROS-induced activation of the DNA damage response pathway as an important mediator of cell-cycle arrest in postnatal cardiomyocytes.

RESULTS

Mitochondrial Characteristics in Neonatal and Zebrafish Hearts

In order to examine the relationship between mitochondrial respiration and regenerative potential in vertebrate hearts amongst species, we first examined mitochondrial DNA content in the ventricular chamber of the heart with quantitative RT-PCR (qRT-PCR) (primers are indicated in Table S1) over 2 weeks after birth in mouse (n = 3) and adult zebrafish (n = 3). Mitochondrial DNA copy number showed a linear increase in the first 2 weeks after birth (Figure 1B, blue bars). Intriguingly, mitochondrial DNA per gram of tissue was low in adult zebrafish and early neonatal mouse hearts (Figure 1B) compared to in the hearts of later postnatal age mice. Next, we examined mitochondrial cristae density, an index of increased proton pumping capacity of mitochondria, in adult zebrafish heart (n = 3) and neonatal mouse hearts (n = 3), using transmission electron microscopy (TEM) imaging. Mitochondrial cristae were sparse in zebrafish and P1 mouse in ventricular cardiomyocytes, but became dense and well-organized at P7 and later postnatal time points (Figure 1C).

To further assess capacity of oxidative metabolism in the postnatal mouse heart, we performed comprehensive mass spectrometry-based quantification of enzymes involved in both aerobic and anaerobic metabolism. We found that the majority of the enzymes related to glycolysis were downregulated from P1 to P7, and concomitantly, the majority of the enzymes involved in mitochondrial Krebs cycle were upregulated in the same time frame (Figure S1A available online). Importantly, over 80% of fatty acid beta oxidation enzymes, the main source of energy in mature cardiomyocytes (Lopaschuk et al., 1994), were upregulated from P1 to P7 (Figure S1A). Finally, we measured mitochondrial NADH oxidase activity, a direct measure of NADH flux through mitochondrial electron transport chain enzymes, and found a significant increase in the same time frame, from P1 to P7 (Figure S1B). These results demonstrate that a precise correlation exists between the regenerative

(top panels, white arrows), whereas at P7 (middle panels) and at P14 (lower panels) both 8-oxoG and pATM showed nuclear localization (colocalized with Hoechst 33258, Ho) indicated by arrows.

(G) Oxidative DNA damage and DDR were induced before P7 in cardiomyocyte. Left panels: representative images of 3D imaging of 8-oxoG staining and the number of 8-oxoG foci per cardiomyocyte. Right panels: western blot and quantification of pATM indicating upregulation of DDR. Cardiac troponin T (TnT) was used to normalize sample loading. Error bars represent SEM. *$p < 0.05$; **$p < 0.01$.

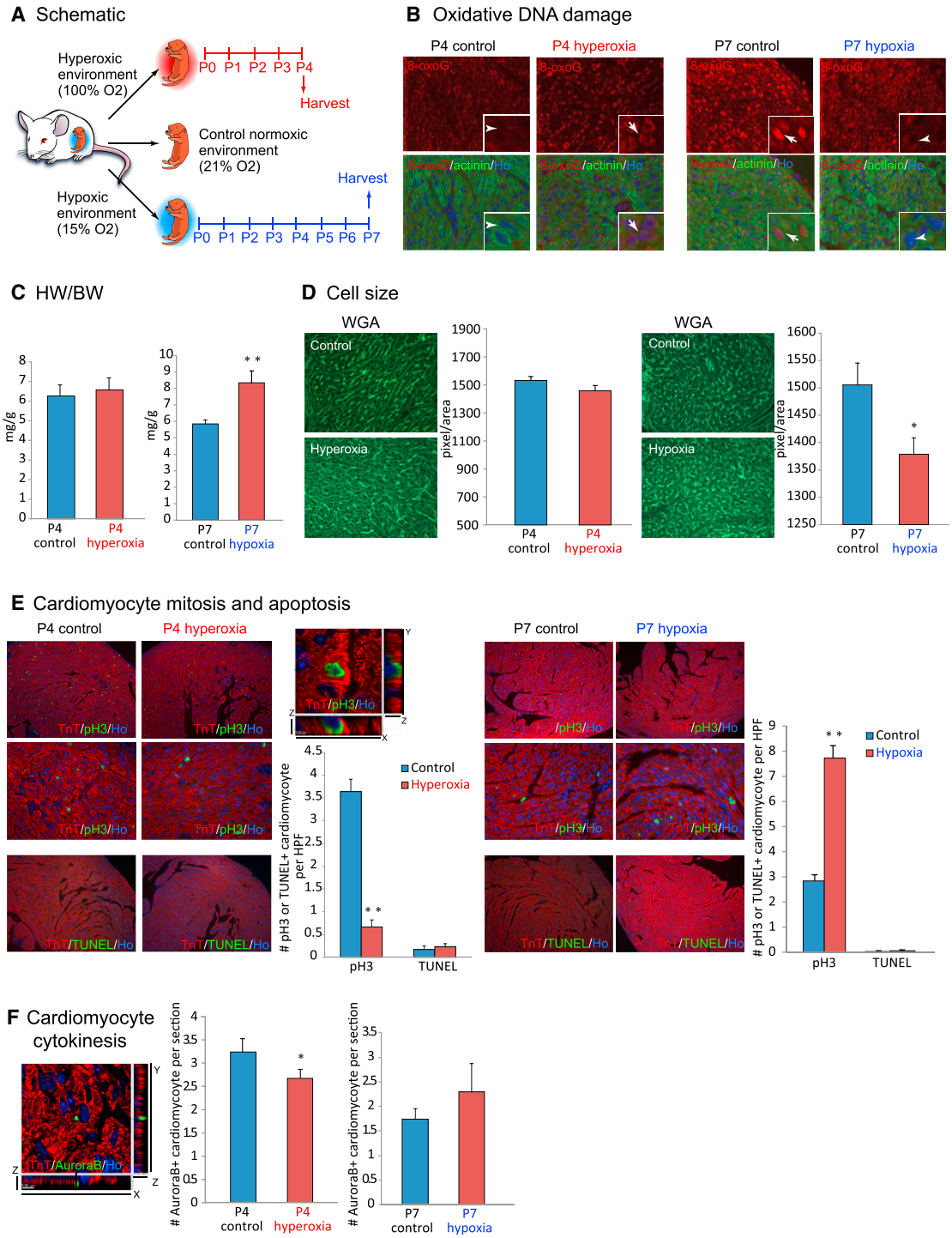

Figure 2. Postnatal Cardiomyocyte Cell-Cycle Arrest Is Dependent on Environmental Oxygen Concentration

(A) Neonates were exposed to hyperoxic (100% O_2) or mildly hypoxic (15% O_2) environment from perinatal stage for 4 days (hyperoxia) or 7 days (hypoxia).

(B) Oxidative DNA damage indicated by nuclear signal with anti-8-oxoG antibody in cardiomyocyte was increased in hyperoxic hearts (left panels) and decreased in hypoxic hearts (right panels).

(C) Heart weight versus body weight (HW/BW) ratio showed no statistically significant difference in mice exposed to hyperoxia, whereas significantly increased in mice exposed to hypoxia.

(D) Cardiomyocyte cell size did not show significant difference in hyperoxia and was decreased in hypoxia.

(legend continued on next page)

zebrafish heart and the early neonatal mouse heart and outline the time frame of the metabolic switch from anaerobic glycolysis to mitochondrial oxidative phosphorylation in mouse heart within one week after birth.

Activation of DNA Damage Response Pathway in Postnatal Mouse Heart

An important byproduct of mitochondrial respiration is the generation of reactive oxygen species (ROS), which cause cellular oxidative stress, in turn inducing various types of cellular toxicity including widespread damage to proteins, lipids, and nucleic acids (Judge and Leeuwenburgh, 2007). We therefore assessed the production of ROS and oxidative stress in postnatal cardiomyocytes. ROS were measured by the detection of dihydroethidium (DHE) oxidation product 2-hydroxyethidine (EOH), which is a marker of superoxide generation, and ethidium (E), which is a marker of hydrogen peroxide (H_2O_2) primarily and other ROS, with high-performance liquid chromatography (HPLC) (Figure 1D) (Zhao et al., 2005). In addition, the fluorescence of ROS indicator dihydrorhodamine 123 (Figure 1E), as well as 2′,7′-dichlorofluorescein (H2DCF) (Figure S1C) (Mills et al., 1998; Sundaresan et al., 1995), further supported the increased ROS levels in cardiomyocytes after birth. Moreover, we found that reduced glutathione (L-γ-glutamyl-L-cysteinylglycine [GSH]) and oxidized glutathione disulfide (GSSG) both decreased progressively from P1 to P4 and further at P7 (Figure S1D). However, GSSG decreased to a greater extent, which resulted in an overall increase in the GSH:GSSH ratio (Figure S1D). Although the ratio of reduced to oxidized glutathione is widely used as an index of oxidative stress (Schafer and Buettner, 2001), recently the absolute levels of GSSG have been shown to exert significant toxic effects. In fact, the decline in the intracellular levels of GSSG is considered a protective mechanism under conditions of oxidative damage. Therefore, in the current study, the age-dependent reduction in GSH and the further reduction in GSSG are strong indicators of the oxidant environment in the postnatal heart, however, it does not seem that there is an overall increased susceptibility to oxidative stress given the elevated GSH:GSSG ratio. We next examined the levels of various antioxidant enzymes by quantitative mass spectrometry. We found that mitochondrial superoxide dismutase (SOD2) (Halliwell and Gutteridge, 2007) was the only antioxidant enzyme that was significantly increased at P4 and P7 compared to P1, while other antioxidant enzymes failed to increase (Figure S1E).

These results led us to hypothesize that oxidative DNA damage caused by ROS may increase in cardiomyocytes postnatally and plays a role in postnatal cell-cycle arrest. Therefore we assessed and quantified oxidative base modification of DNA (8-oxo-7,8-dihydroguanine [8-oxoG]). We found that nuclear 8-oxoG was undetectable at P1, but significantly increased at P7 and P14 (Figure 1F, left panels). In concert, DNA damage response pathway was significantly activated as indicated by upregulation of phosphorylated ataxia telangiectasia mutated (pATM), an essential mediator of DNA damage response activation, at P7 and P14 (Figure 1F, right panels). In addition, further analysis of nuclear 8-oxoG using high resolution confocal microscopy and quantification of oxidized DNA damage foci revealed a significant increase in the number of oxidized DNA damage foci at P4 and P7 compared to P1 (Figure 1G). Also, quantitative analysis of nuclear pATM by western blot showed a significant increase in levels as early as P4, with further increase at P7 compared to P1 (Figure 1G). Furthermore, qRT-PCR analysis for downstream effectors of the DNA damage response pathway also confirmed upregulation of other DNA damage response components including genes involved in damaged DNA binding and repair (Figure S1F). Interestingly, we found that ATM mRNA was mildly downregulated, despite the significant upregulation of the active phosphorylated form of ATM. Moreover, and consistent with our previous findings, 8-oxoG was not detectable in zebrafish cardiomyocytes (Figure S2). These results demonstrate that the increase in mitochondrial respiration corresponds temporally with an increase in ROS in the neonatal heart and activation of DNA damage response.

Environmental Oxygen Regulates Postnatal Cardiomyocyte Cell-Cycle Arrest

To directly test that whether inspired oxygen can influence postnatal cardiomyocyte cell-cycle arrest, we exposed neonates to hyperoxic (100% O_2) or mildly hypoxic (15% O_2) environment starting at E18.5 (n = 3 each, Figure 2A). Remarkably, oxidative DNA damage and activation of DDR were accelerated in P4 hyperoxia heart, and in contrast, were repressed in P7 hypoxia heart (Figure 2B). We found that heart weight to body weight (HW/BW) ratio was normal in neonates under hyperoxia, but significantly increased in those under hypoxia (Figure 2C). Cell size quantification showed a significant decrease in cardiomyocyte cell size after hypoxia treatment, although hyperoxic treatment did not change the size (Figure 2D). The presence of phosphorylated histone H3 Ser 10 (pH3), a marker of G2-M progression, was significantly decreased in cardiomyocyte after hyperoxia treatment and in contrast increased after hypoxia treatment (Figure 2E). In addition, localization of Aurora B kinase at the cleavage furrow, a marker for cytokinesis, was decreased in hyperoxic hearts and mildly increased in hypoxic hearts (Figure 2F). These results strongly indicate that postnatal oxygen concentration directly affects cardiomyocyte proliferation.

Reactive Oxygen Species Induce Postnatal Cardiomyocyte Cell-Cycle Arrest

To assess the contribution of oxidative stress to cell-cycle arrest of postnatal cardiomyocyte, we injected the ROS generator diquat (5 mg/kg) daily for 3 days after birth (n = 3, Figure 3A). Strong induction of oxidative DNA damage indicated

(E) Coimmunostaining with anti-phosphohistone H3 Ser10 (pH3) and anti-cardiac Troponin T (TnT) antibodies showed drastic decrease in cardiomyocyte mitosis in hyperoxia-exposed hearts, and in contrast, significant increase in cardiomyocyte mitosis in hypoxia-exposed hearts. Cardiomyocyte apoptosis did not increase in either treatment as shown by TUNEL staining.

(F) Coimmunostaining with anti-Aurora B and antisarcomeric actinin antibodies showed decreased cytokinesis in hyperoxic hearts, whereas mild increase in hypoxic hearts. Error bars represent SEM. *$p < 0.05$; **$p < 0.01$.

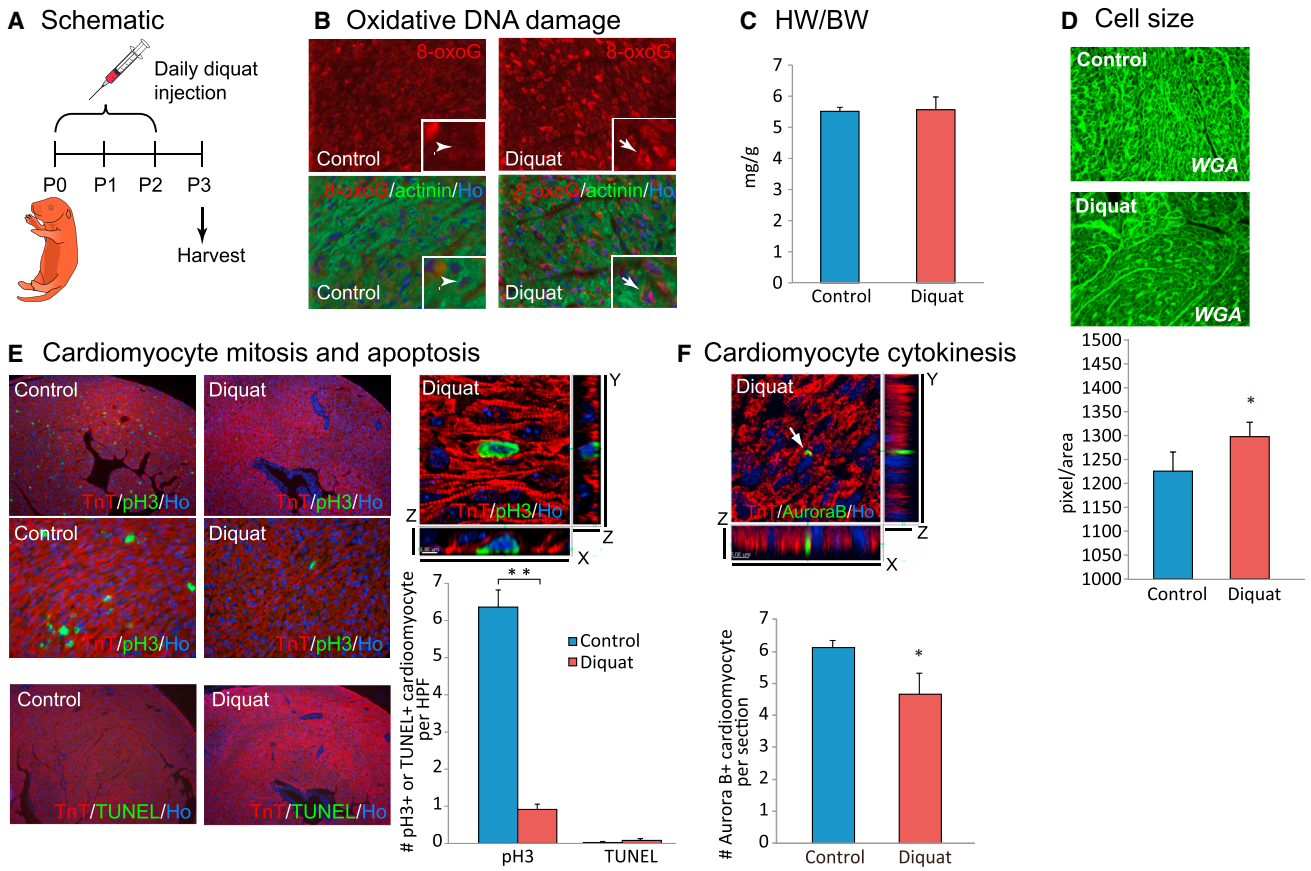

Figure 3. Injection of ROS Generator Diquat Induced Accelerated Cardiomyocyte Cell-Cycle Arrest

(A) Diquat (5 mg/kg) was injected subcutaneously for 3 days after birth and hearts were harvested at P3.

(B) Immunostaining showed nuclear accumulation of 8-oxoG in cardiomyocytes in diquat injected neonates.

(C) HW/BW ratio has no statistically significant difference.

(D) WGA staining showed significantly increased cardiomyocyte cell size in hearts of diquat injected neonates.

(E) Coimmunostaining with anti-pH3 and anti-TnT antibodies showed drastic decrease in cardiomyocyte mitosis in diquat-injected hearts. TUNEL assay showed no significant increase in cardiomyocyte apoptosis.

(F) Diquat injection resulted in decreased cardiomyocyte cytokinesis as shown by coimmunostaining with anti-Aurora B, anti-TnT antibodies. Error bars represent SEM. *$p < 0.05$; **$p < 0.01$.

by 8-oxoG (Figure 3B) was observed, and although HW/BW ratio was unchanged (Figure 3C), we found that the size of individual cardiomyocytes was significantly increased (Figure 3D). In addition, cardiomyocyte mitosis assessed by anti-pH3 staining was drastically reduced in cardiomyocytes in the diquat injected neonates (Figure 3E). TUNEL assay showed no increase in apoptotic cell death (Figure 3E). Finally, cardiomyocyte cytokinesis assessed by anti-Aurora B staining was also significantly decreased in the hearts of diquat injected neonates (Figure 3F). These finding were further confirmed with the injection of another ROS generator paraquat (5 mg/kg, n = 3, Figure S3A). The injection of paraquat induced an increase in cardiomyocyte cell size (Figure S3B) and a decrease in cardiomyocyte mitosis, without significant increase in apoptosis (Figure S3C). Cardiomyocyte cytokinesis was consistently decreased with paraquat injection (Figure S3D). Moreover, we directly injected 30 μl of 1 μM H_2O_2 into the apex of P1 mouse hearts (n = 3, Figure S4A). Two days after H_2O_2 injection, strong induction of phosphorylated ATM was observed (Figure S4B), and although heart weight to body weight ratio was in normal range (Figure S4C), the size of individual cardiomyocytes was significantly increased (Figure S4D). In addition, cardiomyocyte mitosis was almost completely lost in the H_2O_2-treated hearts throughout the entire myocardium (Figure S4E). Although a significant increase in apoptotic cardiomyocyte cell death was shown in the direct H_2O_2-injected hearts, the vast majority of the TUNEL positive cells were along the needle track, while the effect on myocyte proliferation was global throughout the myocardium (Figure S4F). In combination, these results strongly indicate that ROS can induce a shift from hyperplastic to hypertrophic growth in the postnatal mammalian heart. It is important to note here that although there is a clear inhibitory effect on cell-cycle in the absence of increased cell death, the physiological relevance if these stimuli is less certain because we are unable to control the amount or cellular localization of ROS production.

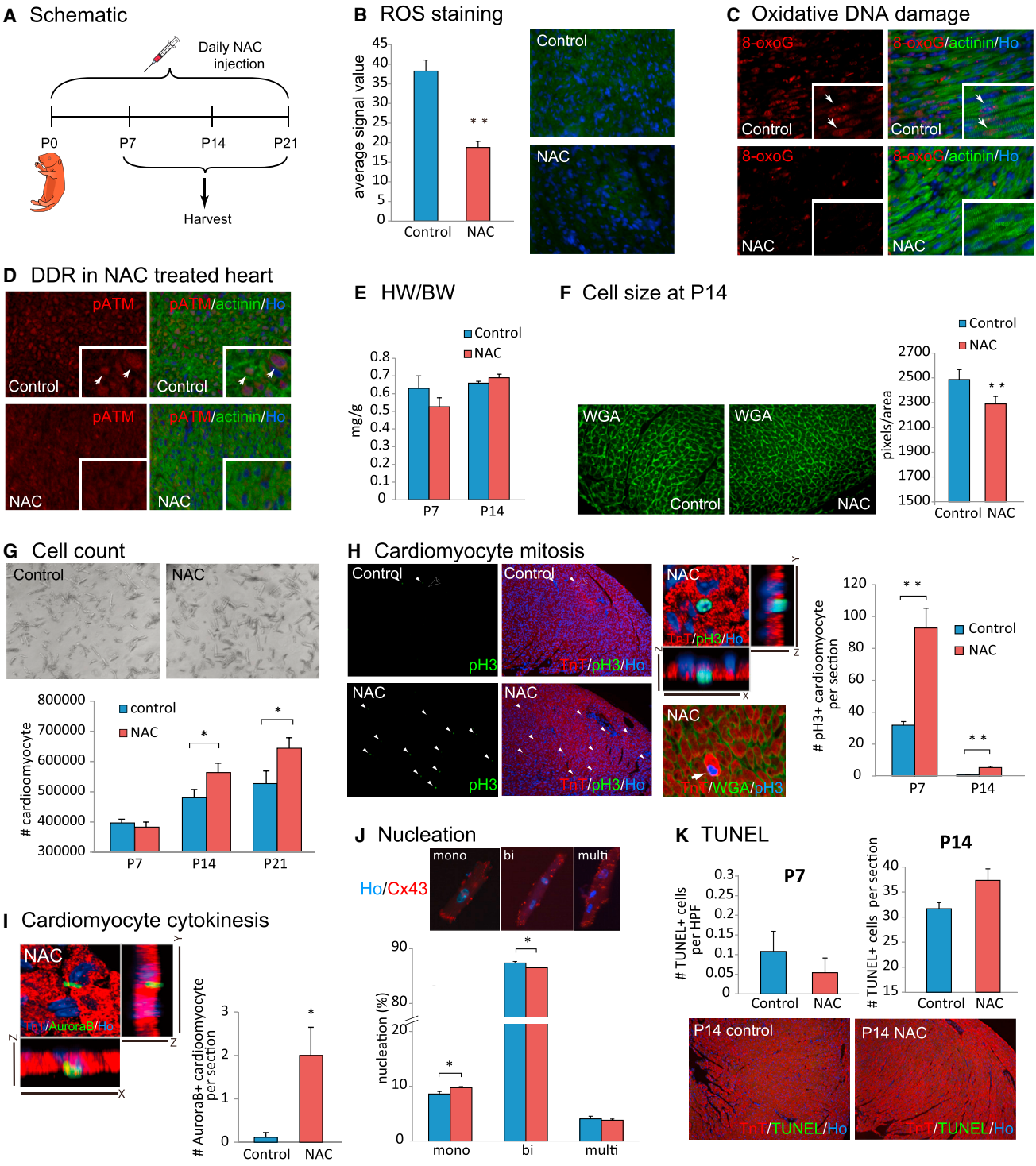

Figure 4. Injection of a Scavenger against ROS Suppresses Postnatal Cardiomyocyte Cell-Cycle Arrest

(A) N-acetyl-cysteine (NAC) was administered for 21 days after birth.

(B) ROS level in cardiomyocytes significantly decreased as shown by dihydrorhodamine 123 staining in NAC-treated neonates.

(C) Reduced 8-oxoG staining was seen in NAC-injected heart, demonstrating reduced oxidative DNA damage in cardiomyocyte at P7.

(D) NAC injection suppressed activation of DNA damage response pathway. Coimmunostaining with anti-pATM and anti-α actinin antibodies showed that NAC treatment reduces nuclear phospho-ATM at P7 compared with control (arrows in left panels).

(E) HW/BW ratio in control and NAC-treated hearts at P14 showed no significant difference.

(F) Cell size quantification using WGA staining showed significantly decreased cell size in NAC-treated hearts.

(legend continued on next page)

Scavenging Reactive Oxygen Species Prolongs Postnatal Cardiomyocyte Proliferation

To test whether scavenging ROS can extend cardiomyocyte proliferation after birth, we administered N-acetylcysteine (NAC) daily for 3 weeks after birth (n = 3, Figure 4A). Staining with dihydrorhodamine 123 showed a decreased cellular ROS level after NAC treatment (Figure 4B). Accordingly, the level of 8-oxoG (Figure 4C) and phosphorylated ATM (Figure 4D) were markedly decreased in cardiomyocyte nuclei after a 1 week treatment with NAC, indicating that oxidative DNA damage and the activation of the DDR by oxidative stress was suppressed. Although HW/BW ratio was normal (Figure 4E), cardiomyocyte cell size was significantly decreased in NAC-treated neonates (Figure 4F). This suggests that NAC treatment delays the postnatal switch from hyperplastic to hypertrophic growth. To confirm this finding, we performed a number of additional studies. First, we observed that NAC treatment increased the total number of cardiomyocytes (Figure 4G). We next examined cardiomyocyte proliferation in NAC-treated hearts. Cardiomyocyte mitosis (Figure 4H) in the NAC-treated hearts compared to control hearts at both P7 and P14 (Figure 4H) and cytokinesis were significantly increased in the NAC-treated hearts (Figure 4I). In addition, we found that the NAC-treated hearts had significantly more mononucleated and less binucleated cardiomyocytes (Figure 4J). Finally, TUNEL assay showed no increase in cell death (Figure 4K). In addition, NAC treatment on isolated neonatal rat cardiomyocytes significantly increased DNA synthesis and mitosis and also reduced polyploidy (Figure S5). However, we noted that cardiomyocyte proliferation gradually decreased over time in the NAC-treated heart within 1 month after birth (data not shown). Detection of the DHE products with HPLC also indicates that both superoxides and other ROS were significantly reduced upon NAC treatment (Figure S6A). qRT-PCR and quantitative mass spectrometry analyses showed little change in levels of proteins involved in oxidative phosphorylation in the NAC-treated p7 hearts compared to control p7 hearts (Figure S6C). The measurement of NADH oxidase activity revealed increase in mitochondrial respiration at P7 even upon NAC administration (Figure S6D). Overall, these results are consistent with a model in which an increase in reactive oxygen species triggers cardiomyocyte cell-cycle arrest shortly after birth.

Mitochondrial-Specific Scavenging of ROS Induces Postnatal Cardiomyocyte Proliferation

To selectively examine whether mitochondrial ROS production is involved in postnatal cell-cycle arrest of cardiomyocytes, we utilized a genetic model to overexpress a radical scavenger specifically in cardiomyocyte mitochondria. We crossed floxed-stop mCAT (mitochondrial-specific catalase) mice, in which floxed transcriptional stop sequences are inserted in between universal GAPDH enhancer/promoter and mCAT (Dai et al., 2011; Schriner et al., 2005), with Myh6-Cre mice to generate mice expressing mCAT only in cardiomyocytes by cardiomyocyte-specific deletion of floxed-stop with Myh6 enhancer/promoter-driven Cre recombinase (hereinafter called mCAT mice, Figure 5A).

We found that ROS levels were decreased in the mCAT hearts by dihydrorhodamine 123 staining (Figure 5B). Quantification of ROS by HPLC detection of EOH peak showed no significant change in the level of superoxide and significant reduction in the E peak, indicative of substantial decrease in H_2O_2 (as expected given that catalase primarily acts on H_2O_2, Figure S6B). Accordingly, oxidative DNA damage (Figure 5C) and the activation of DDR pathway (Figure S6E) were suppressed. In mCAT mice, HW/BW ratio was normal (Figure 5D), however, cardiomyocyte cell size in mCAT mice at P14 was significantly smaller than that in control mice (Figure 5E). In addition, cardiomyocyte mitosis (Figure 5F), as well as cytokinesis (Figure 5G), were increased in mCAT hearts. Accordingly, the total number of cardiomyocyte in mCAT mice was significantly increased in comparison with that in control mice (Figure 5H). The number of proliferative mononucleated cardiomyocytes was increased and binucleated cardiomyocytes were decreased in mCAT heart (Figure 5I). Cardiomyocyte apoptosis was in the normal range in mCAT heart (Figure 5J). These results indicate that mitochondrial ROS production induces postnatal cell-cycle arrest of cardiomyocytes.

NAC Injection Improves Cardiac Function after Injury

We next tested whether ROS scavenging can extend the regenerative potential of mammalian heart. We injected NAC daily after birth and induced ischemia reperfusion (IR) injury at P21 (n = 12), a time point well beyond the P7 where the postnatal heart loses its regenerative potential (Figure 6A). It is important to note here that the control mice also received NAC at the time of IR injury to equalize any effect of NAC injection of ROS-induced infarct expansion following ischemia reperfusion. Cardiomyocyte viability assessed with 2,3,5-trimethyl tetrazolium chloride (TTC) staining was not significantly different between long-term NAC-treated and control hearts (n = 3, Figure 6B). One week and 1 month after the IR injury, there was no significant change in heart size in the NAC-treated animals (Figure 6C). WGA staining showed a significant decrease in cardiomyocyte cell size at 1 month after IR injury, which along with the unchanged HW/BW suggests that the NAC-treated hearts have more cardiomyocytes (Figure 6D). In addition, systolic function was significantly improved in the NAC-treated group (Figure 6E). Fibrotic

(G) Total number of cardiomyocyte was significantly increased in NAC-treated heart at P21.

(H) Coimmunostaining with anti-pH3 and anti-TnT antibodies showed increased cardiomyocyte mitosis in NAC-treated hearts. Images shown are hearts from PBS-injected control or NAC-injected neonates at P14.

(I) NAC injection induced cardiomyocyte cytokinesis indicated by Aurora B and TnT double-positive cardiomyocytes.

(J) Percentage of binucleated cardiomyocytes was significantly decreased and mononucleation was significantly increased in NAC-treated hearts at P14. Immunocytochemistry on isolated myocyte with anti-Cx43 antibody and Hoechst 33258 (Ho) nuclear-specific dye were used to visualize boundary and nuclei of each cardiomyocyte, respectively.

(K) Apoptotic cell death visualized with TUNEL assay was not increased in NAC-treated heart at neither P7 nor P14. Error bars represent SEM. *$p < 0.05$; **$p < 0.01$.

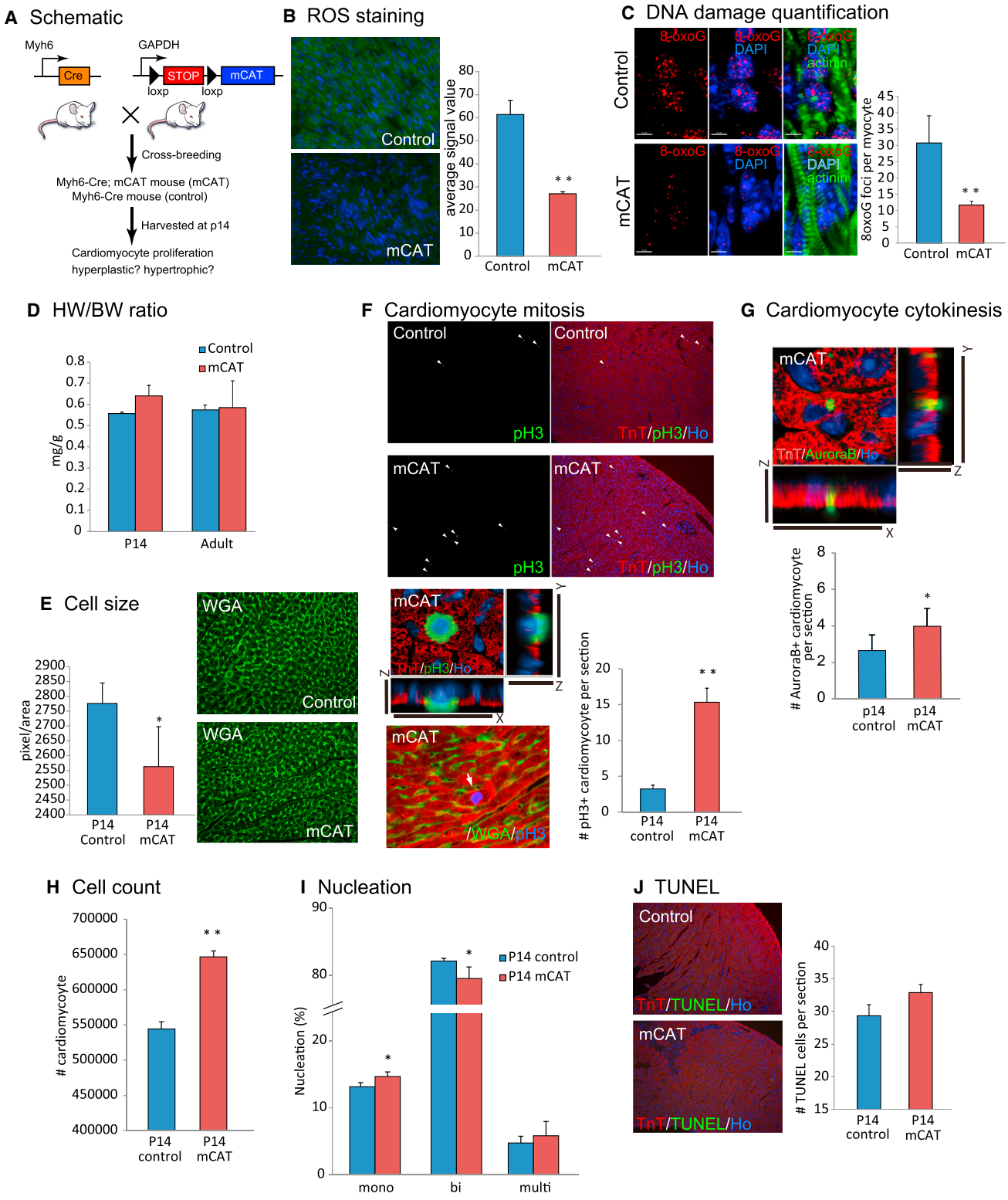

Figure 5. Scavenging Reactive Oxygen Species in Mitochondria Suppresses Postnatal Cardiomyocyte Cell-Cycle Arrest

(A) Mitochondrial-targeted catalase (mCAT) was overexpressed in cardiomyocyte by flipping floxed-stop cassette between GAPDH promoter and mCAT by crossing with mice harboring Myh6 promoter driven Cre recombinase. Myh6-Cre; floxed-stop mCAT mice are hereinafter called mCAT mice. Litter-mate Myh6-Cre mice were used as control.

(legend continued on next page)

scar formation was also decreased after NAC treatment (Figure 6F). Finally, by assessing the number of pH3 positive cardiomyocyte at 3 days after IR (Figure 6G) and BrdU incorporation into cardiomyocytes nuclei at 7 days after IR (Figure 6H), we showed that cardiomyocyte proliferation was significantly increased in the NAC-treated hearts. These data indicate that scavenging ROS can extend regenerative potential of the heart beyond 1 week after birth. It is important here to note that there may be several effects of NAC going on concomitantly; for example, although we administered NAC to the control group for a short period of time after injury in an attempt counteract any effect of NAC on ROS-mediated reperfusion injury, it is likely that the continued NAC administration over 1 month also resulted in decreased cardiomyocyte loss and remodeling following injury.

Pharmacological Inhibition of DNA Damage Response Pathway Extends the Window of Cardiomyocyte Proliferation in the Postnatal Mouse Heart

In order to determine whether DNA damage-induced activation of cell-cycle checkpoint pathway is involved in cardiomyocytes cell-cycle arrest, we examined the Wee1-dependent activation of G2-M cell-cycle checkpoint in postnatal cardiomyocytes. Activation of ATM or ATR kinase in response to DNA damage in turn activates Wee1 kinase, a repressor of CDK1-dependent G2-M transition (Figure 7A) (Heald et al., 1993; Parker and Piwnica-Worms, 1992; Santamaría et al., 2007). We found that nuclear Wee1 was absent from cardiomyocyte nuclei immediately after birth, but became strongly expressed at P7 as well as P14 (Figure 7B, left). Western blot confirmed the increased in Wee1 at p4 and further at P7 (Figure 7B, right). To test whether Wee1 plays a role in postnatal cardiomyocyte cell-cycle arrest, we injected Wee1 inhibitor MK-1775 daily from birth until 2 weeks of age (n = 3, Figure 7C). Wee1 inhibition resulted in a trend toward decrease in heart size, which was not statistically significant (Figure 7D). Notably, Wee1 inhibitor-treated hearts showed robust induction of cardiomyocyte proliferation at P14 indicated by both anti-pH3 (Figure 7E) and anti-Aurora B (Figure 7G) immunostaining, as well as reduced cardiomyocyte cell size (Figure 7F). TUNEL assay showed no increase in apoptotic cell death in Wee1 inhibitor-treated hearts (Figure 7H). Moreover, total number of cardiomyocytes in Wee1 inhibitor-treated P14 hearts was significantly increased both at P7 and at P14 (Figure 7I), and cardiomyocyte binucleation was inhibited (Figure 7J). Furthermore, Wee1 was downregulated when ROS was scavenged in NAC injected or mCAT mice (Figure S6B) at P7. These results suggest that Wee1 mediates postnatal cardiomyocyte cell-cycle arrest and that blocking Wee1 kinase is sufficient to extend the postnatal proliferative window.

In summary, our results indicate that a postnatal increase in mitochondrial-derived reactive oxygen species induces cell-cycle arrest through activation of the DNA damage response pathway in mouse heart within 7 days after birth. Moreover, it is intriguing that the oxidation status and regenerative capacity are well correlated among regenerative lower vertebrates and the early postnatal mammalian heart.

DISCUSSION

One of the long-standing mysteries in cardiovascular biology is the permanent cell-cycle arrest of adult cardiomyocytes, both from an etiological as well as mechanistic perspective. From a mechanistic perspective, several regulators of cardiomyocyte cell cycle have been identified (Agah et al., 1997; Bersell et al., 2009; Chen et al., 2013; Eulalio et al., 2012; Jackson et al., 1990; Liao et al., 2001; Liu et al., 2010; Mahmoud et al., 2013; Porrello et al., 2011a; Reiss et al., 1996; Sdek et al., 2011; Xin et al., 2013) including both direct and indirect cell-cycle regulators. However, the upstream event that triggers these cascades is unknown. A more important question is why are adult cardiomyocytes unable to re-enter cell cycle on demand, for example after injury? In the current report, we show that the increase in environmental oxygen, and the subsequent upregulation of oxidative metabolism, is the upstream signal that triggers cell-cycle exit of cardiomyocytes shortly after birth.

We provide multiple levels of evidence to support our hypothesis that increased environmental oxygen, with the subsequent increase in mitochondrial oxidative metabolism, induces cardiomyocyte cell-cycle arrest through activation of the DNA damage response. First, we show that the regenerative zebrafish heart, similar to the early postnatal mouse heart, has very low mitochondrial content and complexity, and shows no evidence of activation of the DDR pathway. Second, we show that the postnatal increase in mitochondrial mass, complexity, and activity, increased ROS, increased markers of DNA damage, and activation of DDR pathway, all correlate temporally with cell-cycle exit of cardiomyocytes. Third, we show that postnatal hypoxemia inhibits DNA damage and prolongs the postnatal window of cardiomyocytes proliferation, while postnatal hyperoxemia potentiates DNA damage and early cell-cycle arrest. Fourth, we show that ROS generators induce DDR and early cell-cycle arrest, while both nonspecific and mitochondrial-targeted ROS scavenging delays activation of the DNA damage response

(B) The level of ROS in cardiomyocyte decreased in mCAT heart compared with control.
(C) mCAT significantly suppressed DNA damage shown by 3D imaging and the quantification of 8-oxoG foci in cardiomyocyte.
(D) HW/BW ratio in control and mCAT mouse hearts at P14 and in the adult was not changed.
(E) WGA staining showed a decrease in cell size in mCAT hearts.
(F) Increased cardiomyocyte mitosis in mCAT mouse hearts at p14 indicated by coimmunostaining with anti-pH3 and anti-troponin T antibodies.
(G) Increase in cardiomyocyte cytokinesis shown by immunostaining with anti-Aurora B antibody.
(H) Total number of cardiomyocyte was significantly increased at P14 in mCAT mouse heart.
(I) Number of binucleated cardiomyocytes was significantly decreased and mononucleated cardiomyocytes was significantly increased in mCAT hearts.
(J) TUNEL positive apoptotic cell death was within normal range in mCAT heart. Error bars represent SEM. *$p < 0.05$; **$p < 0.01$.

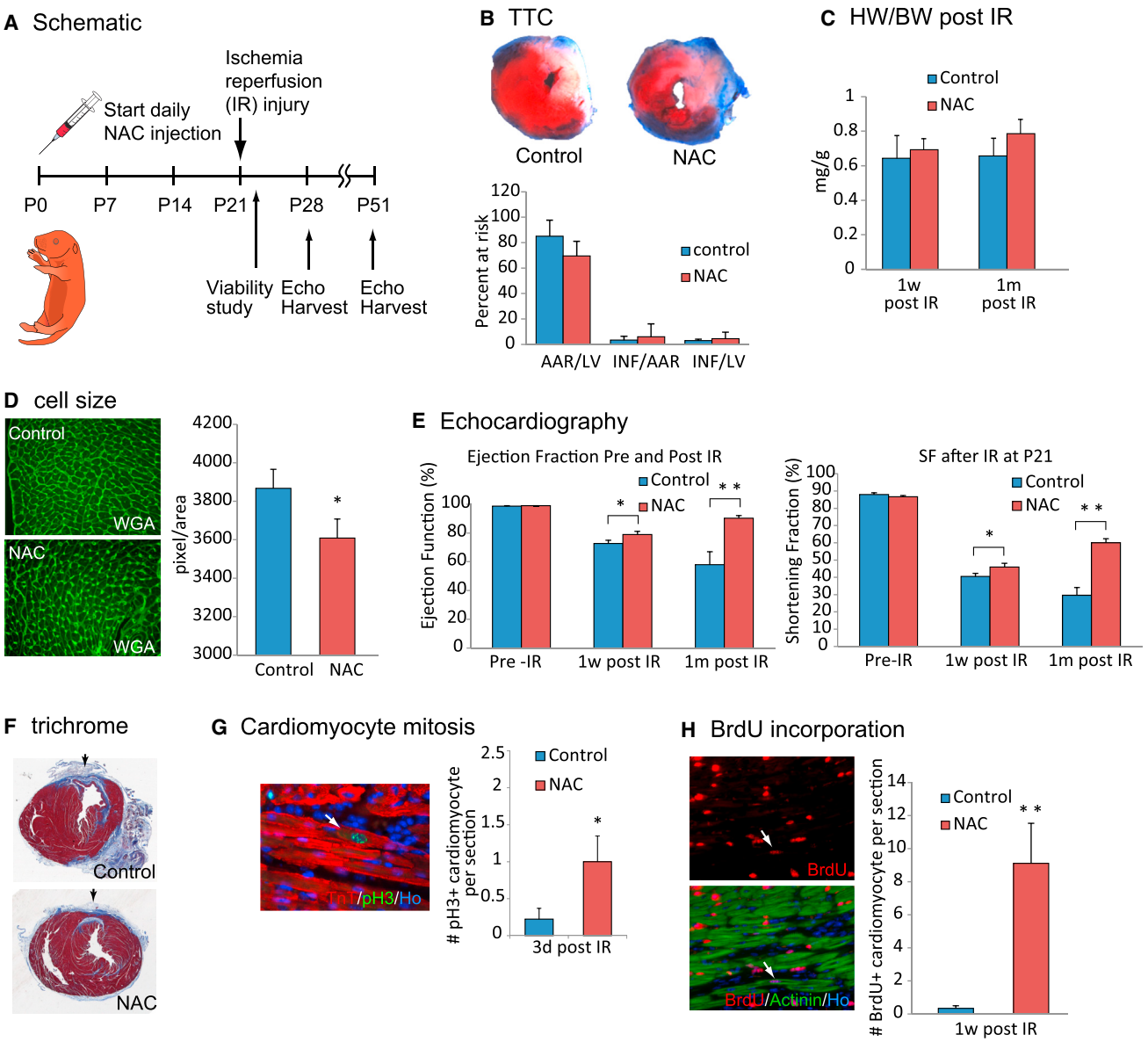

Figure 6. Scavenging ROS Extends Postnatal Cardiac Regeneration Window

(A) Animals were treated with NAC from P0 and subjected to ischemia reperfusion (IR) surgery at P21. Viability was investigated 24 hr after injury to evaluate the consistency of the IR surgery, and cardiac function was examined by echocardiography at 1 week and 1 month after injury.

(B) TTC staining showed no significant difference in the size of injury between control and NAC-pretreated hearts.

(C) HW/BW ratio at 1 week or 1 month after IR surgery between control and NAC-pretreated mice was not changed.

(D) WGA staining showed a decrease in cell size in NAC-treated hearts 1 month after IR injury compared to control hearts, indicating the NAC treatment did not induce cardiomyocyte hypertrophy.

(E) Left ventricular systolic function quantified by ejection fraction (EF) and shortening fraction (SF) (n = 6 per group) before IR surgery (left), 1 week after surgery (middle), and 1 month after surgery (right) showed more functional recovery in NAC-pretreated hearts compared with control hearts.

(F) Histological analysis with Masson trichrome staining showed reduced fibrotic scar formation in NAC-treated hearts.

(G) Cardiomyocyte mitosis was increased in NAC-treated mice as indicated by anti-pH3 and anti-TnT coimmunostaining at 3 days after IR injury.

(H) Immunostaining with anti-BrdU and anti-Actinin antibodies showed increased cardiomyocyte BrdU incorporation in NAC-pretreated heart. Error bars represent SEM. *p < 0.05; **p < 0.01.

and delays cell-cycle arrest of cardiomyocytes. Finally, we show that pharmacological inhibition of the DDR pathway prolongs the postnatal window of cardiomyocyte proliferation. It is important to note here that although we were able to prolong the postnatal window of myocyte proliferation with ROS scavenging, we were unable to prevent cell-cycle arrest. The inevitable cell-cycle exit of cardiomyocyte is likely multifactorial and possibly related to our inability to completely prevent DNA damage, or other factors

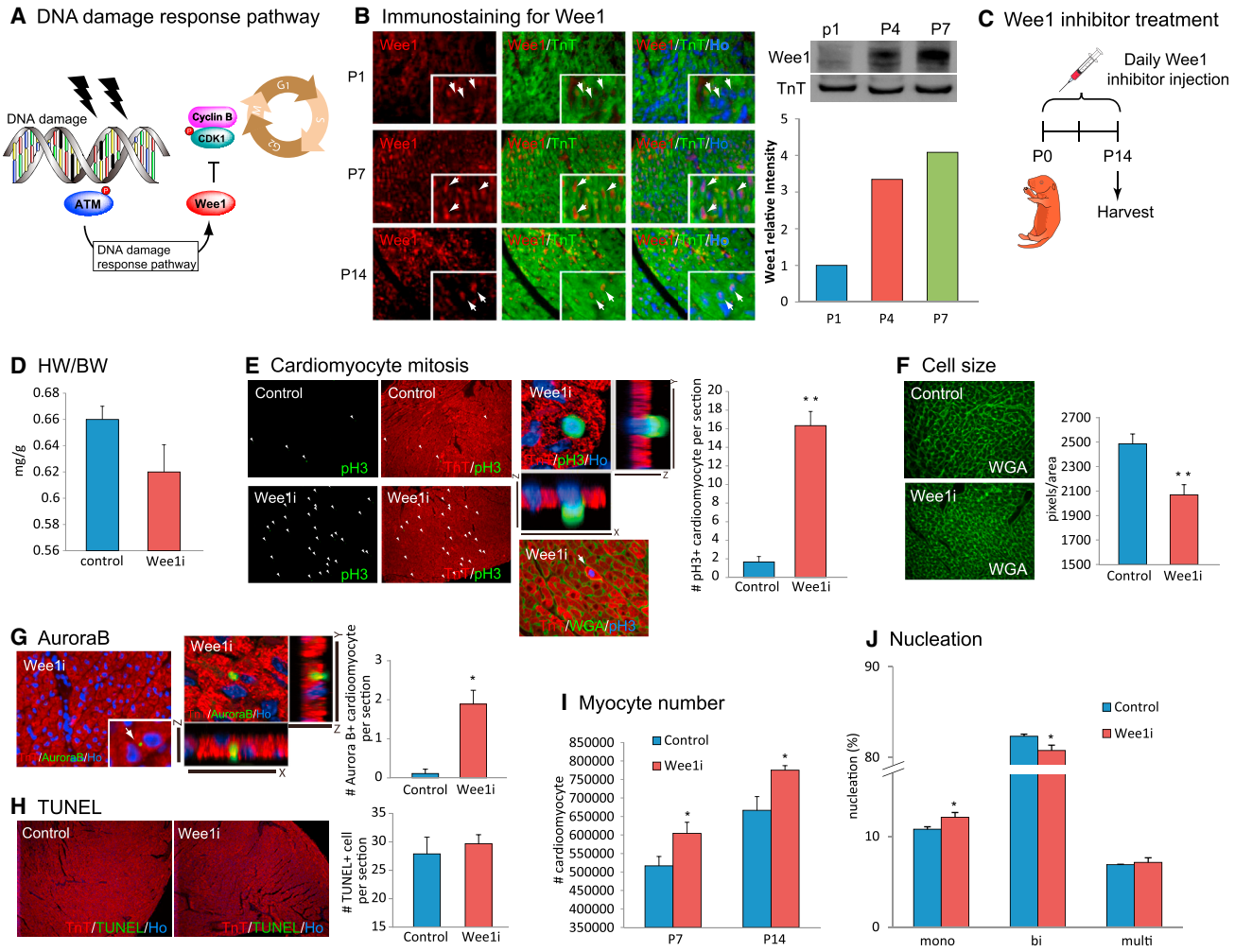

Figure 7. Inhibition of an Effector of DNA Damage Response, Wee1 Kinase, Suppresses Postnatal Cardiomyocyte Cell-Cycle Arrest

(A) DNA damage response pathway activates Wee1 kinase that inhibits cell cycle regulator Cyclin/CDKs, resulting in cell-cycle arrest.

(B) Immunostaining with anti-Wee1 and anti-TnT antibodies showed no expression of Wee1 protein in cardiomyocytes at P1 (arrows), and then nuclear localized Wee1 protein at P7 and P14 (arrows).

(C) Daily injection of Wee1 kinase inhibitor MK-1775 was performed from birth until P14.

(D) Wee1 inhibitor injection resulted in slight, but not statistically significant, decrease in HW/BW ratio compared with control.

(E) Inhibition of Wee1-induced mitosis in cardiomyocyte at P14 shown by pH3/TnT immunostaining.

(F) Quantification of cell size with WGA staining showed decreased cardiomyocyte size in Wee1 inhibitor-treated hearts.

(G) AuroraB/TnT immunostaining showed increased cardiomyocyte cytokinesis in Wee1 inhibitor-treated hearts.

(H) No increase in apoptotic cell death in cardiomyocyte indicated by TUNEL assay.

(I) Total number of cardiomyocyte was increased at P7 and P14 in Wee1 inhibitor-treated hearts.

(J) Number of binucleated cardiomyocytes was reduced, and mononucleated cardiomyocyte was increased in Wee1 inhibitor-treated heart. Error bars represent SEM. *$p < 0.05$; **$p < 0.01$.

such as the postnatal change in type and abundance of nutrients (Siggens et al., 2012) or increased hemodynamic stress. Similarly, pharmacological inhibition of Wee1 delayed, but did not prevent, cell-cycle arrest. This is, perhaps, not surprising given the downstream cell-cycle targets of the DDR pathway that do not involve Wee1, which regulates cyclin B/CDK1, while cyclin E/CDK2 is targeted by other components of the DDR pathways.

The effect of ROS on cell cycle is complex and probably greatly influenced by level, source, type, compartmentalization, and duration of exposure to ROS. Evidence suggests that ROS can be proproliferative in several scenarios (Leslie, 2006; Tothova et al., 2007) and can stimulate differentiation of several cell types (Lee et al., 2005; Owusu-Ansah and Banerjee, 2009; Tsatmali et al., 2006) including cardiomyocytes. In vitro studies using embryonic stem (ES) cells have shown that redox balance is a critical regulator of cardiomyocyte differentiation (Birket et al., 2013). ROS mediates mechanical strain and electrical stimulation-induced cardiomyocyte differentiation of ES cells (Pucéat et al., 2003), while ROS scavengers impair cardiomyocyte formation in embryoid bodies (Pi et al., 2013; Sauer

et al., 2000; Yoneyama et al., 2010). In contrast, ROS-mediated senescence and cell-cycle exit is a well-recognized characteristic of stem cells (Takahashi et al., 2006; Trachootham et al., 2009).

The current report demonstrates that the neonatal mouse heart and the zebrafish heart may have more in common than previously recognized. The hypoxic nature of the zebrafish external and circulatory environments prevents activation of the DDR and cell-cycle arrest of myocytes. In support of this notion, additional hypoxia actually enhances myocyte proliferation and regenerative capacity of zebrafish hearts (Jopling et al., 2012; Marques et al., 2008) and in the current report, prolongs the postnatal window of myocyte proliferation in mammals. Shortly after birth, the metabolic switch that occurs in the mammalian heart confers significant energy efficiency through oxidative metabolism, unfortunately at the expense of proliferative competency. We conclude that mitochondrial ROS-mediated activation of the DDR is an important upstream event that mediates cell-cycle arrest of postnatal cardiomyocytes.

EXPERIMENTAL PROCEDURES

Animal Breeding and Genotyping

All protocols were approved by the Institutional Animal Care and Use Committee of the University of Texas Southwestern Medical Center (UTSW). All experiments were performed on age- and sex-matched mice, with equal ratio of male to female mice. The number of animals used for each experiment; n = 3. Transgenic mCAT mice were kindly provided by Dr. Ravinovitch. Mice were genotyped as described previously (Dai et al., 2011; Schriner et al., 2005).

Drug Injection

N-acetyl-L-cysteine (NAC, Sigma) was reconstituted in PBS to concentrations of 10 mg/ml. CD-1 (Charles River) mice were weighed daily and 75 mg/kg of NAC was injected daily subcutaneously or intraperitoneal from day 0 to day 14. Wee1-inhibitors (MK-1775, Selleck) were reconstituted in diluted DMSO. CD-1 mice were injected daily with 2.5 mg/kg subcutaneously or intraperitoneal from day 0 to day 14. Diquat, paraquat, and H_2O_2 were diluted in PBS and injected into CD-1 neonates as described in Results.

Histology

Hearts were harvested and fixed in 4% paraformaldehyde (PFA)/PBS solution overnight at room temperature and then processed for paraffin sectioning. Masson's trichrome staining was performed according to standard procedures at UTSW core histology facility on paraffin sections. TUNEL staining was performed according to manufacturer's recommendations (In Situ Cell Death Detection Kit, Fluorescein, catalog number 11684795910, Roche).

Immunostaining

Following antigen retrieval with 1 mM EDTA in boiling water, sections were blocked with 10% serum from host animal of secondary antibodies, and incubated with primary antibodies overnight at 4°C. Sections were subsequently washed with PBS and incubated with corresponding secondary antibodies conjugated to Alexa Fluor 350, 488, or 555 (Invitrogen). Primary antibodies used are following: anti-phospho Histone H3 Ser10 (Millipore 06-570, 1:100), anti-Aurora B (Sigma A5102, 1:100), anti-Troponin T, Cardiac Isoform Ab-1, Clone 13-11 (Thermo Scientific MS-295-P1, 1:100), anti-Bromodeoxyuridine (Roche 11170376001, 1:25), anti-Sarcomeric Alpha Actinin (Abcam, ab68167, 1:100), anti-Oxoguanine 8 (Abcam Ab64548, 1:100), anti-phosphorylated ATM (Santa Cruz Biotechnology sc-47739, 1:100), anti-Wee1 (Abcam ab137377, 1:100), and anti-wheat germ agglutinin (WGA) conjugated to Alexa Fluor 488 (50 μg/ml, Invitrogen).

Cardiomyocyte Isolation

The isolation of cardiomyocyte from neonatal hearts and staining with anticonnexin 43 antibody were performed as previously described (Mahmoud et al., 2013).

Reactive Oxygen Species Determination

Dihydrorhodamine 123 (Life Technologies, D-23806) or CM-H2DCFDA (Life Technologies, C6827) and HPLC detection of DHE were used to detect ROS. See Extended Experimental Procedures for detailed methods.

Cristae Measurement

Spacings between cristae in individual mitochondria were quantified using ImageJ. Only mitochondria with several well-defined, parallel cristae were selected for analysis. The ImageJ line tool was used to draw a line across the stack of cristae, perpendicular to the orientation of the cristae, and the number of cristae crossing the line was counted interactively. The pixel size defined in the image metadata was used to obtain the length of the line profile in μm.

Western Blotting

Western blot was performed using standard protocols. See Extended Experimental Procedures for detailed methods.

Statistical Analysis

One-tailed or two-tailed Student's t test was used to determine statistical significance and $^*p < 0.05$ and $^{**}p < 0.01$ was considered statistically different. All quantification is blinded.

SUPPLEMENTAL INFORMATION

Supplemental Information includes Extended Experimental Procedures, six figures, and one table and can be found with this article online at http://dx.doi.org/10.1016/j.cell.2014.03.032.

AUTHOR CONTRIBUTIONS

B.N.P. and W.K. designed and performed experiments, analyzed data, made the figures, and wrote the paper. S.A.M., J.M., D.G., R.C., C.X.S., S.W.T., E.M., P.M.R., S.Z., S.M., and A.I.M. performed experiments. J.F.A., K.L.P., B.A.R., J.A.G., M.T.K., D.J.C., M.G., P.S.R., A.A., A.M.S., and L.I.S. designed and supervised experiments and edited the paper. H.S. conceived the study, designed the experiments, and wrote the paper.

ACKNOWLEDGMENTS

We thank Dr. James Richardson and John Shelton for their valuable input. This work is supported by National Aeronautics and Space Administration (NASA) grant NNX13AD57G (A.A.), Advanced grant 20090506 from the European Research Council (ERC) (M.G.), the British Heart Foundation and a Fondation Leducq Transatlantic Network (A.M.S.), as well as grants from the American Heart Association (Grant in Aid), Foundation for Heart Failure Research (NY), and the NIH (grant 1R01HL115275-01) (H.A.S.).

Received: October 22, 2013
Revised: February 17, 2014
Accepted: March 21, 2014
Published: April 24, 2014

REFERENCES

Agah, R., Kirshenbaum, L.A., Abdellatif, M., Truong, L.D., Chakraborty, S., Michael, L.H., and Schneider, M.D. (1997). Adenoviral delivery of E2F-1 directs cell cycle reentry and p53-independent apoptosis in postmitotic adult myocardium in vivo. J. Clin. Invest. *100*, 2722–2728.

Becker, R.O., Chapin, S., and Sherry, R. (1974). Regeneration of the ventricular myocardium in amphibians. Nature *248*, 145–147.

Bergmann, O., Bhardwaj, R.D., Bernard, S., Zdunek, S., Barnabe-Heider, F., Walsh, S., Zupicich, J., Alkass, K., Buchholz, B.A., Druid, H., et al. (2009). Evidence for cardiomyocyte renewal in humans. Science *324*, 98–102.

Bersell, K., Arab, S., Haring, B., and Kühn, B. (2009). Neuregulin1/ErbB4 signaling induces cardiomyocyte proliferation and repair of heart injury. Cell *138*, 257–270.

Birket, M.J., Casini, S., Kosmidis, G., Elliott, D.A., Gerencser, A.A., Baartscheer, A., Schumacher, C., Mastroberardino, P.G., Elefanty, A.G., Stanley, E.G., et al. (2013). PGC-1alpha and reactive oxygen species regulate human embryonic stem cell-derived cardiomyocyte function. Stem Cell Rep. *1*, 560–574.

Chen, J., Huang, Z.P., Seok, H.Y., Ding, J., Kataoka, M., Zhang, Z., Hu, X., Wang, G., Lin, Z., Wang, S., et al. (2013). mir-17-92 cluster is required for and sufficient to induce cardiomyocyte proliferation in postnatal and adult hearts. Circ. Res. *112*, 1557–1566.

Dai, D.F., Johnson, S.C., Villarin, J.J., Chin, M.T., Nieves-Cintrón, M., Chen, T., Marcinek, D.J., Dorn, G.W., 2nd, Kang, Y.J., Prolla, T.A., et al. (2011). Mitochondrial oxidative stress mediates angiotensin II-induced cardiac hypertrophy and Galphaq overexpression-induced heart failure. Circ. Res. *108*, 837–846.

Dawes, G.S., Mott, J.C., and Widdicombe, J.G. (1954). The foetal circulation in the lamb. J. Physiol. *126*, 563–587.

Dismukes, G.C., Klimov, V.V., Baranov, S.V., Kozlov, Y.N., DasGupta, J., and Tyryshkin, A. (2001). The origin of atmospheric oxygen on Earth: the innovation of oxygenic photosynthesis. Proc. Natl. Acad. Sci. USA *98*, 2170–2175.

Eulalio, A., Mano, M., Dal Ferro, M., Zentilin, L., Sinagra, G., Zacchigna, S., and Giacca, M. (2012). Functional screening identifies miRNAs inducing cardiac regeneration. Nature *492*, 376–381.

Fisher, D.J., Heymann, M.A., and Rudolph, A.M. (1980). Myocardial oxygen and carbohydrate consumption in fetal lambs in utero and in adult sheep. Am. J. Physiol. *238*, H399–H405.

Flink, I.L. (2002). Cell cycle reentry of ventricular and atrial cardiomyocytes and cells within the epicardium following amputation of the ventricular apex in the axolotl, Amblystoma mexicanum: confocal microscopic immunofluorescent image analysis of bromodeoxyuridine-labeled nuclei. Anat. Embryol. (Berl.) *205*, 235–244.

Gertz, E.W., Wisneski, J.A., Stanley, W.C., and Neese, R.A. (1988). Myocardial substrate utilization during exercise in humans. Dual carbon-labeled carbohydrate isotope experiments. J. Clin. Invest. *82*, 2017–2025.

González-Rosa, J.M., Martín, V., Peralta, M., Torres, M., and Mercader, N. (2011). Extensive scar formation and regression during heart regeneration after cryoinjury in zebrafish. Development *138*, 1663–1674.

Halliwell, B., and Gutteridge, J. (2007). Free Radicals in Biology and Medicine (Oxford, UK: Oxford University Press).

Heald, R., McLoughlin, M., and McKeon, F. (1993). Human wee1 maintains mitotic timing by protecting the nucleus from cytoplasmically activated Cdc2 kinase. Cell *74*, 463–474.

Hoeijmakers, J.H. (2009). DNA damage, aging, and cancer. N. Engl. J. Med. *361*, 1475–1485.

Hsieh, P.C., Segers, V.F., Davis, M.E., MacGillivray, C., Gannon, J., Molkentin, J.D., Robbins, J., and Lee, R.T. (2007). Evidence from a genetic fate-mapping study that stem cells refresh adult mammalian cardiomyocytes after injury. Nat. Med. *13*, 970–974.

Jackson, T., Allard, M.F., Sreenan, C.M., Doss, L.K., Bishop, S.P., and Swain, J.L. (1990). The c-myc proto-oncogene regulates cardiac development in transgenic mice. Mol. Cell. Biol. *10*, 3709–3716.

Jopling, C., Suñé, G., Faucherre, A., Fabregat, C., and Izpisua Belmonte, J.C. (2012). Hypoxia induces myocardial regeneration in zebrafish. Circulation *126*, 3017–3027.

Judge, S., and Leeuwenburgh, C. (2007). Cardiac mitochondrial bioenergetics, oxidative stress, and aging. Am. J. Physiol. Cell Physiol. *292*, C1983–C1992.

Koopman, W.J., Nijtmans, L.G., Dieteren, C.E., Roestenberg, P., Valsecchi, F., Smeitink, J.A., and Willems, P.H. (2010). Mammalian mitochondrial complex I: biogenesis, regulation, and reactive oxygen species generation. Antioxid. Redox Signal. *12*, 1431–1470.

Laflamme, M.A., Myerson, D., Saffitz, J.E., and Murry, C.E. (2002). Evidence for cardiomyocyte repopulation by extracardiac progenitors in transplanted human hearts. Circ. Res. *90*, 634–640.

Lawrence, J., Xiao, D., Xue, Q., Rejali, M., Yang, S., and Zhang, L. (2008). Prenatal nicotine exposure increases heart susceptibility to ischemia/reperfusion injury in adult offspring. J. Pharmacol. Exp. Ther. *324*, 331–341.

Lee, N.K., Choi, Y.G., Baik, J.Y., Han, S.Y., Jeong, D.W., Bae, Y.S., Kim, N., and Lee, S.Y. (2005). A crucial role for reactive oxygen species in RANKL-induced osteoclast differentiation. Blood *106*, 852–859.

Leslie, N.R. (2006). The redox regulation of PI 3-kinase-dependent signaling. Antioxid. Redox Signal. *8*, 1765–1774.

Liao, H.S., Kang, P.M., Nagashima, H., Yamasaki, N., Usheva, A., Ding, B., Lorell, B.H., and Izumo, S. (2001). Cardiac-specific overexpression of cyclin-dependent kinase 2 increases smaller mononuclear cardiomyocytes. Circ. Res. *88*, 443–450.

Liu, Z., Yue, S., Chen, X., Kubin, T., and Braun, T. (2010). Regulation of cardiomyocyte polyploidy and multinucleation by CyclinG1. Circ. Res. *106*, 1498–1506.

Lopaschuk, G.D., Collins-Nakai, R.L., and Itoi, T. (1992). Developmental changes in energy substrate use by the heart. Cardiovasc. Res. *26*, 1172–1180.

Lopaschuk, G.D., Belke, D.D., Gamble, J., Itoi, T., and Schönekess, B.O. (1994). Regulation of fatty acid oxidation in the mammalian heart in health and disease. Biochim. Biophys. Acta *1213*, 263–276.

Mahmoud, A.I., Kocabas, F., Muralidhar, S.A., Kimura, W., Koura, A.S., Thet, S., Porrello, E.R., and Sadek, H.A. (2013). Meis1 regulates postnatal cardiomyocyte cell cycle arrest. Nature *497*, 249–253.

Marnett, L.J., Riggins, J.N., and West, J.D. (2003). Endogenous generation of reactive oxidants and electrophiles and their reactions with DNA and protein. J. Clin. Invest. *111*, 583–593.

Marques, I.J., Leito, J.T., Spaink, H.P., Testerink, J., Jaspers, R.T., Witte, F., van den Berg, S., and Bagowski, C.P. (2008). Transcriptome analysis of the response to chronic constant hypoxia in zebrafish hearts. J. Comp. Physiol. B *178*, 77–92.

Mills, E.M., Takeda, K., Yu, Z.X., Ferrans, V., Katagiri, Y., Jiang, H., Lavigne, M.C., Leto, T.L., and Guroff, G. (1998). Nerve growth factor treatment prevents the increase in superoxide produced by epidermal growth factor in PC12 cells. J. Biol. Chem. *273*, 22165–22168.

Miquel, J., Economos, A.C., Fleming, J., and Johnson, J.E., Jr. (1980). Mitochondrial role in cell aging. Exp. Gerontol. *15*, 575–591.

Mitchell, J.A., and Van Kainen, B.R. (1992). Effects of alcohol on intrauterine oxygen tension in the rat. Alcohol. Clin. Exp. Res. *16*, 308–310.

Moos, P.J., Edes, K., and Fitzpatrick, F.A. (2000). Inactivation of wild-type p53 tumor suppressor by electrophilic prostaglandins. Proc. Natl. Acad. Sci. USA *97*, 9215–9220.

Nadal-Ginard, B. (2001). [Generation of new cardiomyocytes in the adult heart: Prospects of myocardial regeneration as an alternative to cardiac transplantation]. Rev. Esp. Cardiol. *54*, 543–550.

Oberpriller, J.O., and Oberpriller, J.C. (1974). Response of the adult newt ventricle to injury. J. Exp. Zool. *187*, 249–253.

Owusu-Ansah, E., and Banerjee, U. (2009). Reactive oxygen species prime Drosophila haematopoietic progenitors for differentiation. Nature *461*, 537–541.

Parker, L.L., and Piwnica-Worms, H. (1992). Inactivation of the p34cdc2-cyclin B complex by the human WEE1 tyrosine kinase. Science *257*, 1955–1957.

Pi, Y., Zhang, L.L., Li, B.H., Guo, L., Cao, X.J., Gao, C.Y., and Li, J.C. (2013). Inhibition of reactive oxygen species generation attenuates TLR4-mediated proinflammatory and proliferative phenotype of vascular smooth muscle cells. Lab. Invest. *93*, 880–887.

Porrello, E.R., Johnson, B.A., Aurora, A.B., Simpson, E., Nam, Y.J., Matkovich, S.J., Dorn, G.W., 2nd, van Rooij, E., and Olson, E.N. (2011a). MiR-15 family regulates postnatal mitotic arrest of cardiomyocytes. Circ. Res. *109*, 670–679.

Porrello, E.R., Mahmoud, A.I., Simpson, E., Hill, J.A., Richardson, J.A., Olson, E.N., and Sadek, H.A. (2011b). Transient regenerative potential of the neonatal mouse heart. Science *331*, 1078–1080.

Porrello, E.R., Mahmoud, A.I., Simpson, E., Johnson, B.A., Grinsfelder, D., Canseco, D., Mammen, P.P., Rothermel, B.A., Olson, E.N., and Sadek, H.A. (2013). Regulation of neonatal and adult mammalian heart regeneration by the miR-15 family. Proc. Natl. Acad. Sci. USA *110*, 187–192.

Poss, K.D., Wilson, L.G., and Keating, M.T. (2002). Heart regeneration in zebrafish. Science *298*, 2188–2190.

Pucéat, M., Travo, P., Quinn, M.T., and Fort, P. (2003). A dual role of the GTPase Rac in cardiac differentiation of stem cells. Mol. Biol. Cell *14*, 2781–2792.

Quaini, F., Urbanek, K., Beltrami, A.P., Finato, N., Beltrami, C.A., Nadal-Ginard, B., Kajstura, J., Leri, A., and Anversa, P. (2002). Chimerism of the transplanted heart. N. Engl. J. Med. *346*, 5–15.

Rees, B.B., Sudradjat, F.A., and Love, J.W. (2001). Acclimation to hypoxia increases survival time of zebrafish, Danio rerio, during lethal hypoxia. J. Exp. Zool. *289*, 266–272.

Reiss, K., Cheng, W., Ferber, A., Kajstura, J., Li, P., Li, B., Olivetti, G., Homcy, C.J., Baserga, R., and Anversa, P. (1996). Overexpression of insulin-like growth factor-1 in the heart is coupled with myocyte proliferation in transgenic mice. Proc. Natl. Acad. Sci. USA *93*, 8630–8635.

Reynolds, J.D., Penning, D.H., Dexter, F., Atkins, B., Hrdy, J., Poduska, D., and Brien, J.F. (1996). Ethanol increases uterine blood flow and fetal arterial blood oxygen tension in the near-term pregnant ewe. Alcohol *13*, 251–256.

Roesner, A., Hankeln, T., and Burmester, T. (2006). Hypoxia induces a complex response of globin expression in zebrafish (Danio rerio). J. Exp. Biol. *209*, 2129–2137.

Rudolph, A.M., and Heyman, M.A. (1974). Fetal and neonatal circulation and respiration. Annu. Rev. Physiol. *36*, 187–207.

Santamaría, D., Barrière, C., Cerqueira, A., Hunt, S., Tardy, C., Newton, K., Cáceres, J.F., Dubus, P., Malumbres, M., and Barbacid, M. (2007). Cdk1 is sufficient to drive the mammalian cell cycle. Nature *448*, 811–815.

Sauer, H., Rahimi, G., Hescheler, J., and Wartenberg, M. (2000). Role of reactive oxygen species and phosphatidylinositol 3-kinase in cardiomyocyte differentiation of embryonic stem cells. FEBS Lett. *476*, 218–223.

Schafer, F.Q., and Buettner, G.R. (2001). Redox environment of the cell as viewed through the redox state of the glutathione disulfide/glutathione couple. Free Radic. Biol. Med. *30*, 1191–1212.

Schriner, S.E., Linford, N.J., Martin, G.M., Treuting, P., Ogburn, C.E., Emond, M., Coskun, P.E., Ladiges, W., Wolf, N., Van Remmen, H., et al. (2005). Extension of murine life span by overexpression of catalase targeted to mitochondria. Science *308*, 1909–1911.

Sdek, P., Zhao, P., Wang, Y., Huang, C.J., Ko, C.Y., Butler, P.C., Weiss, J.N., and Maclellan, W.R. (2011). Rb and p130 control cell cycle gene silencing to maintain the postmitotic phenotype in cardiac myocytes. J. Cell Biol. *194*, 407–423.

Semenza, G.L. (2007). Life with oxygen. Science *318*, 62–64.

Siggens, L., Figg, N., Bennett, M., and Foo, R. (2012). Nutrient deprivation regulates DNA damage repair in cardiomyocytes via loss of the base-excision repair enzyme OGG1. FASEB J. *26*, 2117–2124.

Soonpaa, M.H., Kim, K.K., Pajak, L., Franklin, M., and Field, L.J. (1996). Cardiomyocyte DNA synthesis and binucleation during murine development. Am. J. Physiol. *271*, H2183–H2189.

Sundaresan, M., Yu, Z.X., Ferrans, V.J., Irani, K., and Finkel, T. (1995). Requirement for generation of H2O2 for platelet-derived growth factor signal transduction. Science *270*, 296–299.

Takahashi, A., Ohtani, N., Yamakoshi, K., Iida, S., Tahara, H., Nakayama, K., Nakayama, K.I., Ide, T., Saya, H., and Hara, E. (2006). Mitogenic signalling and the p16INK4a-Rb pathway cooperate to enforce irreversible cellular senescence. Nat. Cell Biol. *8*, 1291–1297.

Tothova, Z., Kollipara, R., Huntly, B.J., Lee, B.H., Castrillon, D.H., Cullen, D.E., McDowell, E.P., Lazo-Kallanian, S., Williams, I.R., Sears, C., et al. (2007). FoxOs are critical mediators of hematopoietic stem cell resistance to physiologic oxidative stress. Cell *128*, 325–339.

Trachootham, D., Alexandre, J., and Huang, P. (2009). Targeting cancer cells by ROS-mediated mechanisms: a radical therapeutic approach? Nat. Rev. Drug Discov. *8*, 579–591.

Tsatmali, M., Walcott, E.C., Makarenkova, H., and Crossin, K.L. (2006). Reactive oxygen species modulate the differentiation of neurons in clonal cortical cultures. Mol. Cell. Neurosci. *33*, 345–357.

Turrens, J.F. (1997). Superoxide production by the mitochondrial respiratory chain. Biosci. Rep. *17*, 3–8.

Turrens, J.F. (2003). Mitochondrial formation of reactive oxygen species. J. Physiol. *552*, 335–344.

Wang, J., Panáková, D., Kikuchi, K., Holdway, J.E., Gemberling, M., Burris, J.S., Singh, S.P., Dickson, A.L., Lin, Y.F., Sabeh, M.K., et al. (2011). The regenerative capacity of zebrafish reverses cardiac failure caused by genetic cardiomyocyte depletion. Development *138*, 3421–3430.

Webster, W.S., and Abela, D. (2007). The effect of hypoxia in development. Birth Defects Res. C Embryo Today *81*, 215–228.

Wisneski, J.A., Gertz, E.W., Neese, R.A., Gruenke, L.D., Morris, D.L., and Craig, J.C. (1985). Metabolic fate of extracted glucose in normal human myocardium. J. Clin. Invest. *76*, 1819–1827.

Xin, M., Kim, Y., Sutherland, L.B., Murakami, M., Qi, X., McAnally, J., Porrello, E.R., Mahmoud, A.I., Tan, W., Shelton, J.M., et al. (2013). Hippo pathway effector Yap promotes cardiac regeneration. Proc. Natl. Acad. Sci. USA *110*, 13839–13844.

Yoneyama, M., Kawada, K., Gotoh, Y., Shiba, T., and Ogita, K. (2010). Endogenous reactive oxygen species are essential for proliferation of neural stem/progenitor cells. Neurochem. Int. *56*, 740–746.

Zhao, H., Joseph, J., Fales, H.M., Sokoloski, E.A., Levine, R.L., Vasquez-Vivar, J., and Kalyanaraman, B. (2005). Detection and characterization of the product of hydroethidine and intracellular superoxide by HPLC and limitations of fluorescence. Proc. Natl. Acad. Sci. USA *102*, 5727–5732.